

Active vibration control of a mounting bracket for automotive gearboxes

D. MAGLIACANO¹, M. CIMINELLO², I. DIMINO², M. VISCARDI¹ and A. CONCILIO²

¹University of Naples "Federico II", Industrial Engineering Department, Napoli

²Adaptive Structures Division, C.I.R.A. – The Italian Aerospace Research Centre, Capua (CE)
ITALY

darius6591@hotmail.it, m.ciminello@cira.it, i.dimino@cira.it, mavisar@unina.it, a.concilio@cira.it

Abstract: - The aim of this paper is to investigate the use of active vibration control in automotive gearboxes mounting brackets to reduce tonal disturbances. A combination of piezoelectric accelerometers and an internally preloaded piezo stack actuator is used to counteract their unbalanced caused vibrations. Initially, a numerical modal analysis was carried out to identify the normal modes in the frequency range of interest. The piezo stack was simulated by a ROD element and its effect numerically characterized. The upper and lower faces of the stack were mechanically coupled with the bracket structure, whereas the active control strategy involved the relative displacement of two opposite points of the bracket. To this aim, dedicated interfaces were designed to integrate the stack into the mounting bracket. In order to control the vibrations in correspondence of the second bending mode (1599.4Hz), the primary disturbance, simulated by a shaker, was modelled in the frequency domain using a white noise signal. A narrow window of 20Hz was initially selected as the control system domain. Then, this frequency range has been made gradually wider around the resonance peak, in order to optimize the control effect, and then extended up to 80 Hz when undesired effects occurred. Primary and secondary control plants were firstly numerically fitted from the measured responses and excitations using system identification techniques, and then used for the active controller design and simulations.

Key-Words: - active vibration control, automotive, gearbox, piezoceramic actuators

1 Introduction

The primary goal of this activity is the development of a control system, based on a piezoceramic device, for the reduction of tones in the 5-2000 Hz range of a mounting bracket for automotive gearboxes. The control is numerically simulated and implemented using the software MSC Nastran. In particular, the studied control system is based on a piezoceramic actuator in the form of a stack which, if suitably integrated in the structure, acts on specific tones of the control range, reducing the width of the structural response due to an excitation of vibrational type.

2 Problem Formulation

From preliminary tests conducted on the system, it appeared that it shows an annoying whistle in third gear linked to a resonance of the bracket. Therefore, it was generated the CAD model of the bracket (Figure 1) and, downstream of the application of appropriate constraint conditions, the studies have concentrated on the said component. In the next images, the shown plan is X-Z, with X that points to the right, Z points upward and Y accordingly, so as

to form a left-handed triad. As already anticipated, the hypothesized solution involves the use of a piezoceramic stack that works to normal effort, whose characteristics are reported in Table 1; the stacks are constituted by a network of piezoceramics, connected mechanically in series and electrically in parallel, which allows the generation of a bigger force compared to piezoelectric patches.

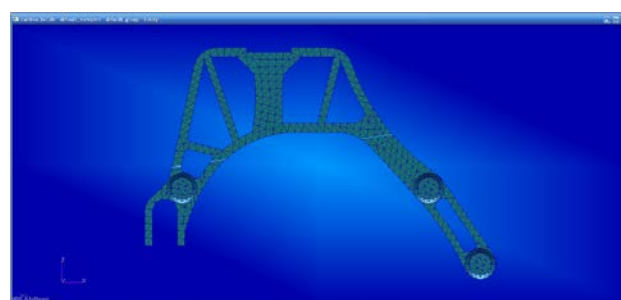


Figure 1: Bracket CAD model

Table 1: Geometrical and mechanical characteristics of the piezoceramic stack

| | |
|---------------|----------|
| Model | P-016.20 |
| Length [mm] | 29 |
| Diameter [mm] | 16 |

| | |
|------------------------------------|----------------------|
| Area [mm ²] | 201.06 |
| Stiffness [Kg/s ²] | 1.83*10 ⁸ |
| Young modulus [N/mm ²] | 4.24*10 ⁷ |
| Density [Kg/mm ³] | 7.8*10 ⁻⁶ |
| Blocking force [N] | 5500 |
| Maximum displacement [μm] | 30 |
| Maximum supply voltage [V] | 1000 |

The graph in Figure 2 was obtained by applying the formula:

$$F = F_b - Ks \quad (1)$$

In particular, by applying the boundary condition:

$$F = 0, s = s_{max} \rightarrow K = \frac{F_b}{s_{max}} \quad (2)$$

It can be calculated the value of the piezoceramic stiffness.

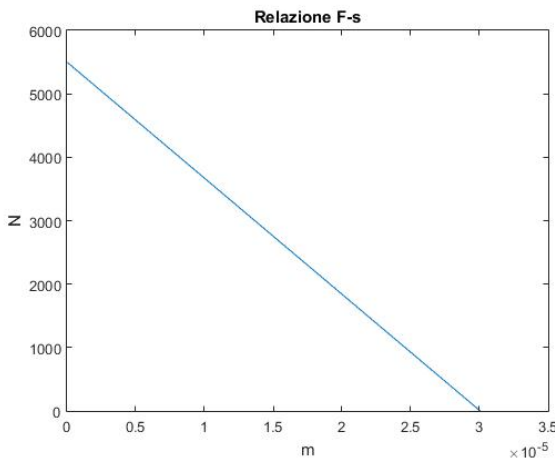


Figure 2: Strength - displacement graph of the piezoceramic stack

2.1 Modal analysis

Initially, it was conducted a numerical modal analysis without the piezoceramic stack, which detected two vibration modes in the 5-2000 Hz range; its results are shown, in terms of displacements and of strain energy, hereinafter in Figures 3, 4, 5 and 6. Note that, since the first mode of vibration is of flexural type and is out of the plane of the bracket, the numerical control through the use of a piezoceramic stack has been developed only in the vicinity of the second mode of vibration, which is instead in the flexional plane of the bracket. Subsequently, it was simulated the piezoceramic stack as a ROD element, with the axis tilted $14^\circ = 0.2443$ rad compared with Z axis (Figure 7). The introduction of this additional item in the structure constitutes a reason of variation of the modal frequencies, whose general expression is:

$$\omega_N = \sqrt{\frac{K}{m}} \quad (3)$$

Downstream of a new modal analysis, that this time takes into account the (passive) presence of the piezoceramic stack, the new modes, in terms of displacements and of strain energy, in Figures 8, 9, 10 and 11. Considering Formula 3 and the results reported in Table 2, it is possible to deduce that the introduction of the said element in the system brings an additional contribution of mass greater than that of stiffness.

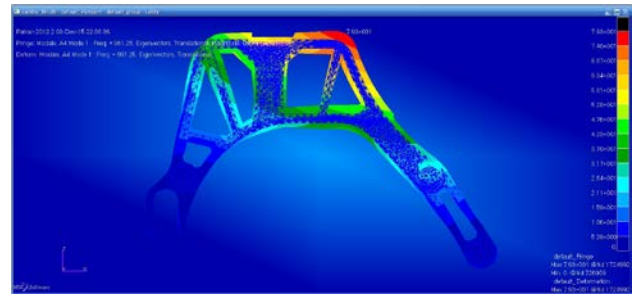


Figure 3: Displacements (without ROD) – mode 1

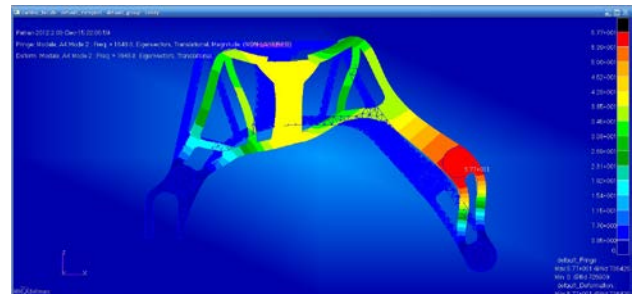


Figure 4: Displacements (without ROD) – mode 2



Figure 5: Strain energy (without ROD) – mode 1

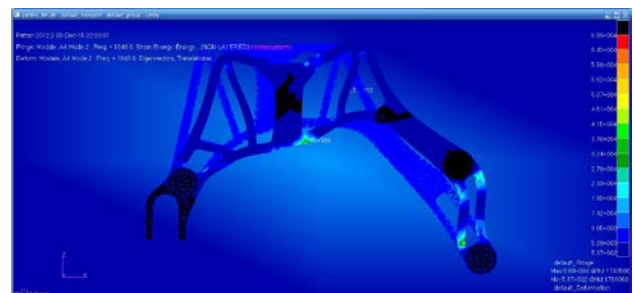


Figure 6: Strain energy (without ROD) – mode 2

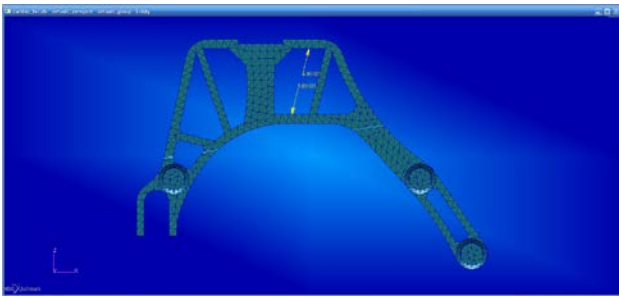


Figure 7: Actuation axis direction of the piezoceramic stack

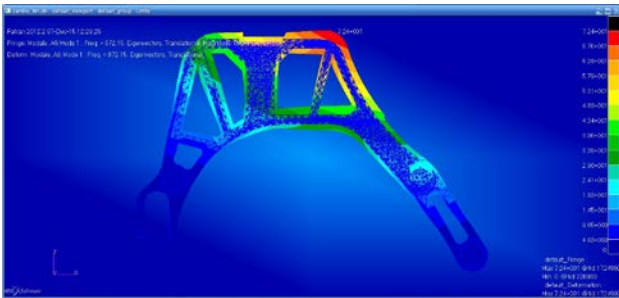


Figure 8: Displacements (with ROD) – mode 1

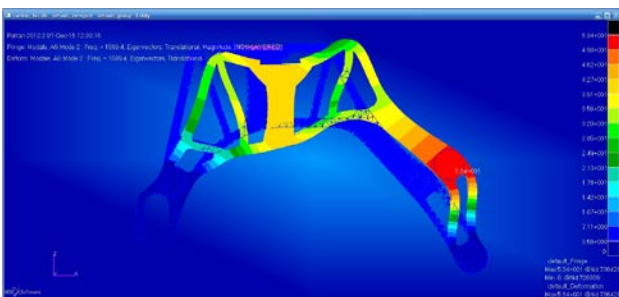


Figure 9: Displacements (with ROD) – mode 2



Figure 10: Strain energy (with ROD) – mode 1

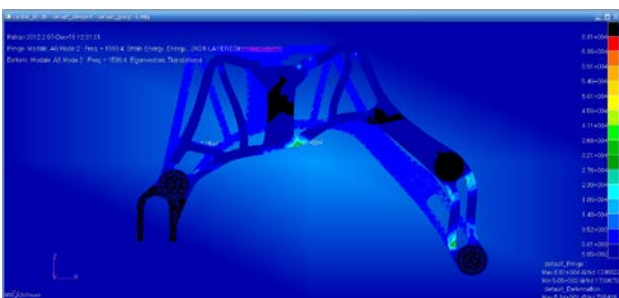


Figure 11: Strain energy (with ROD) – mode 2

Table 2: Modal frequencies with and without the presence of the ROD element

| | Mode I | Mode II |
|-------------|-----------|-----------|
| Without ROD | 961.25 Hz | 1648.8 Hz |
| With ROD | 872.15 Hz | 1599.4 Hz |

2.1.1 Considerations

Note that a cylindrical device with both faces placed at points of the structure (as well as the used piezoceramic stack), cannot effectively control absolute magnitudes such as the displacement, the speed or the acceleration of a point of the structure: in fact it exerts a normal force along both directions of its axis and therefore, in an attempt to control the displacement of a point adjacent to the upper face of the stack, it may increase (in dependence on the structure thicknesses of the two contact surfaces and on the relative phase shift between them) that of the point adjacent to the lower face. Instead, a control device such as that described is suitable to the deformation control, thought as the relative displacement between two points belonging respectively to the two contact surfaces, and therefore the following analysis was carried out in order to reduce this size.

2.2 Comparison between direct and modal FRF techniques

In order to implement the control system, some FRFs in various configurations have been conducted; the MSC Nastran software offers the possibility to perform frequency response analysis using a direct or a modal technique. The latter, in particular, intrinsically constitutes an approximation of the first one, but offers considerable advantages in terms of computational cost. It was therefore conducted a preliminary comparison, exciting the structure with an acceleration along Z equal to 1 g, applied in the left and in the lower right corner bolts, and detecting the response in terms of acceleration of a particular point of the structure (Figure 12) calculated with both techniques; as shown in Table 3, the difference between the values obtained is definitely negligible and therefore this has allowed to calculate all subsequent FRFs using the modal technique.

Table 3: Comparison between direct and modal FRF results

| | X [mm/s ²] | Y [mm/s ²] | Z [mm/s ²] |
|--------|------------------------|------------------------|------------------------|
| Direct | 3,8905*10 ³ | 1,8245*10 ³ | 6,8606*10 ³ |

| | | | |
|-------|---------------------|---------------------|---------------------|
| Modal | $3,8906 \cdot 10^3$ | $1,8247 \cdot 10^3$ | $6,8601 \cdot 10^3$ |
|-------|---------------------|---------------------|---------------------|

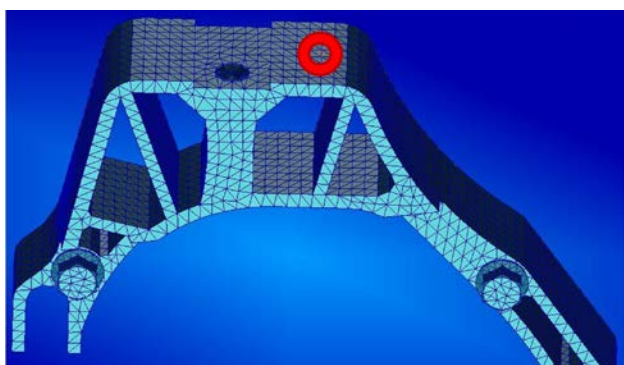


Figure 12: Control point for the FRF comparison

2.3 Control system implementation

The primary excitation that simulates the effect of a shaker, equal to 1 g, directed along Z and applied in correspondence of the left and the lower right bolts, is modeled in frequency as a white noise. A white noise is a particular type of noise, characterized by the absence of time periodicity and by constant amplitude over the whole spectrum of frequencies of interest; it is called "white" due to the analogy with the fact that a similar electromagnetic radiation spectrum within the range of visible light would appear to the human eye as a white light. In order to control the deformation in the vicinity of the second mode of vibration, it is opted to implement the control at a frequency of 1599.4 Hz, introducing a damping of 1% of the critical one. For this specific frequency value, it is calculated the phase to optimize the control using the formula:

$$\text{Control phase [deg]} = 180 - (B2 - B1) \quad (4)$$

Where:

- B1 is the phase of the excitation device – sensor FRF;
 - B2 is the phase of the control device – sensor FRF.
- In particular, the tonal response is calculated in terms of deformation between two points located on the two opposite faces of the piezoceramic, first only due to the excitation of the shaker ($a = 1 \text{ g}$, $\varphi = 0^\circ$) and then solely due to the effect of the stack ($F = 1 \text{ N}$, $\varphi = 0^\circ$). Downstream of the reasoning set out above, two key numbers regarding the piezoceramic stack have been calculated:
- The module of the control force to be applied in order to completely cancel the deformation at a specific frequency, equal to 1.629 N; alternatively, the application of a unit force in any case produces a remarkable result, breaking down the uncontrolled response of 70% (in other words, of -10.5 dB).
 - The optimum phase of the control force, reported in Table 4.

Table 4: Piezoceramic stack control phase

| | |
|-----------------------|------------------|
| Shaker response phase | 256.3573° |
| Stack response phase | 354.3934° |
| Control phase | 81.9639° |

3 Results

Initially, as shown in Figures 13 and 14, the range of frequencies in which to study the effect of the control was chosen equal to 20 Hz (1590 Hz - 1610 Hz); within that range, the control action has constant amplitude and phase, chosen to optimize the specific resonance conditions at 1599.4 Hz. Subsequently, it was extended the frequency range of application of the control (in a differentiated manner for $F = 1 \text{ N}$ and $F = 1.629 \text{ N}$), in order to best control the "bell" of the resonance peak, without varying amplitude and phase of the control force; the results of this operation are visible in Figures 15 and 16. By further extending the control frequency range (1560 Hz - 1640 Hz, Figures 17 and 18), as expected, an unwanted effect is produced, since doing so a disturbance (for effect of the piezoceramic stack) it's introduced at the frequencies to which the external excitation (which was modeled on the control action) is negligible compared to the effect of the control itself. In conclusion, the optimal frequency ranges in which to extend the control are:

- $F = 1 \text{ N} \rightarrow 1576 \text{ Hz} - 1624 \text{ Hz}$
- $F = 1.629 \text{ N} \rightarrow 1582 \text{ Hz} - 1615 \text{ Hz}$

The result plots are shown, expressed both in linear and logarithmic scale; the black line shows the uncontrolled response, the red one is the control using $F = 1 \text{ N}$ and lastly the blue one corresponds to the controlled response with $F = 1,629 \text{ N}$.

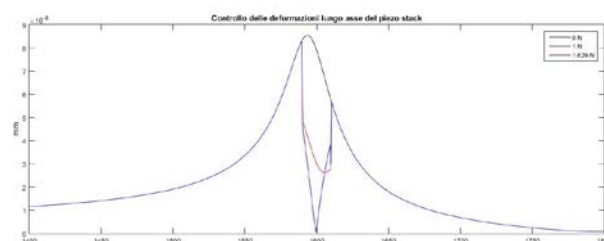


Figure 13: Control on a 20 Hz range, linear graph

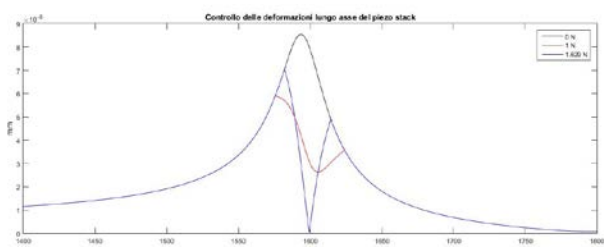


Figure 14: Optimal control, linear graph

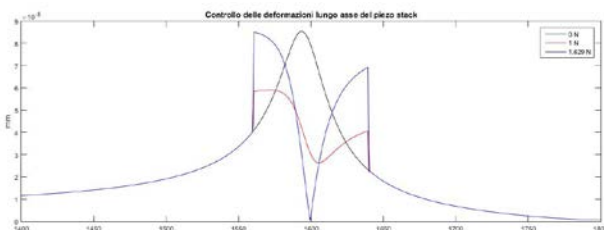


Figure 15: Control on an 80 Hz range, linear graph

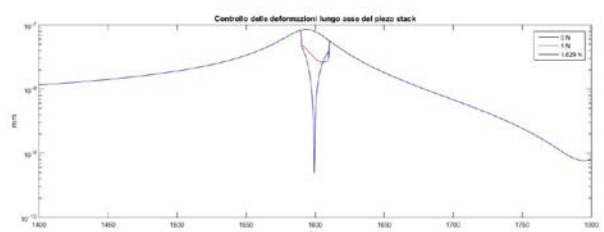


Figure 16: Control on a 20 Hz range, logarithmic graph

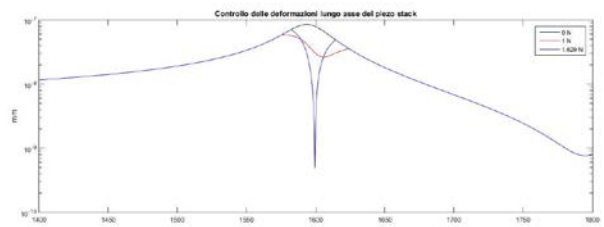


Figure 17: Optimal control, logarithmic graph

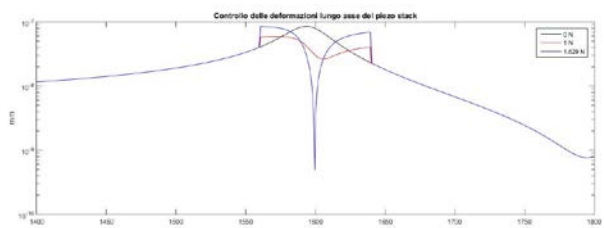


Figure 18: Control on an 80 Hz range, logarithmic graph

angular interfaces (Figure 19) and two FRFs between 1300 Hz and 1800 Hz were acquired, respectively generated from the shaker (Figure 20) and the piezoceramic stack (Figure 21). Evidently, the resonance frequencies are different and more numerous than those identified by the numerical analysis: this can be explained by the additional presence of the two angular interfaces. The experimental resonance nearest to the numeric one is at about 1580 Hz; this makes it probably the best candidate around which carry out experimental control tests necessary to validate the numerical model discussed.

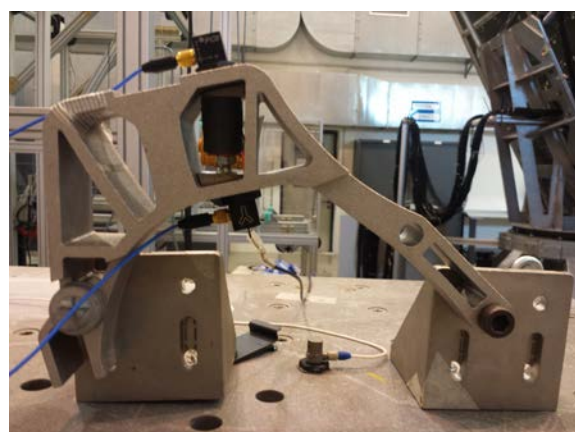


Figure 19: Bracket with stack installed on the shaker; in correspondence of the piezoceramic, two accelerometers are visible

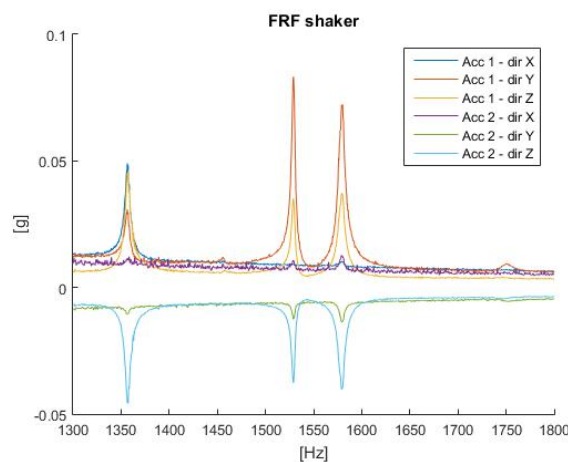


Figure 20: Frequency response function generated by the shaker

4 Conclusion: experimental activity

As conclusion, it is shown the principle of experimental work which will then be conducted on the bracket of the gearbox; in particular, the bracket was installed on the shaker of the C.I.R.A. vibro-acoustic testing laboratory through the use of two

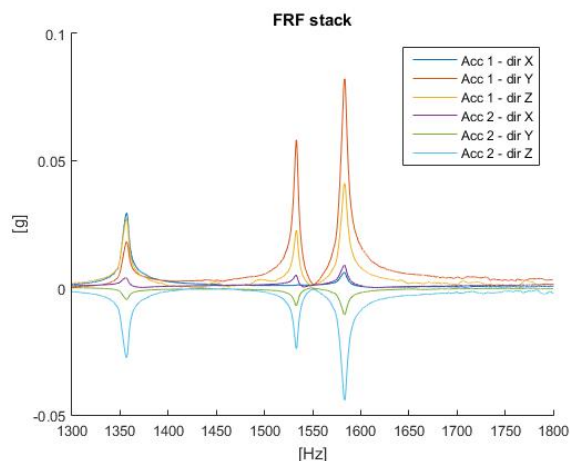


Figure 21: Frequency response function generated by the piezoceramic stack

References

- 1 Preumont, K. Seto; *Active Control of Structures*; Wiley; 2008.
- 2 S. Leleu, H. Abou-Kandil, Y. Bonnassieux; *Piezoelectric actuators and sensors location for active control of flexible structures*; *IEEE Transactions on Instrumentation and Measurement (Volume:50, Issue: 6)*; 2002.
- 3 Viscardi, M., & Lecce, L. (2002). *An integrated system for active vibro-acoustic control and damage detection on a typical aeronautical structure*. Paper presented at the IEEE Conference on Control Applications - Proceedings, Retrieved from www.scopus.com
- 4 Lecce, L., Viscardi, M., Zumpano, G.; *Multifunctional system for active noise control and damage detection on a typical aeronautical structure* - Proceedings of SPIE - The International Society for Optical Engineering, 4327, pp. 201-212. DOI: 10.1117/12.436531
- 5 D. Magliacano; *Controllo attivo di rumore e vibrazioni in ambito automotive*; Università degli Studi di Napoli "Federico II"; 2016.
- 6 F. Svaricek, T. Fueger, H. Karkosch, P. Marienfeld and C. Bohn; *Automotive Applications of Active Vibration Control*; University of the German Armed Forces Munich, Technical University Clausthal.